Express Polymer Letters Vol.18, No.10 (2024) 991–1007
Available online at www.expresspolymlett.com
https://doi.org/10.3144/expresspolymlett.2024.76

Research article

Sustainable ZnO nanoparticles using sweet lime peel extract: Eco-friendly activator in rubber for tire applications

Sreethu Thiyyanthiruthy Kumbalaparambil, Ajay Haridas Chandaparambil, Kinsuk Naskar[*]

Rubber Technology Centre, Indian Institute of Technology Kharagpur, 721302, West Bengal, India

Received 29 April 2024; accepted in revised form 8 July 2024

Abstract. This study addresses the increasing demand for eco-friendly rubber compounding additives by exploring green-synthesized zinc oxide (ZnO) nanoparticles. The green synthesis of ZnO nanoparticles is gaining attention due to its eco-friendly approach and potential applications. This study investigates the synthesis of ZnO nanoparticles using sweet lime peel extract as a green method, comparing it with chemical synthesis. The obtained nanoparticles are characterized and evaluated for suitability as activators in natural rubber composites for tire applications. Furthermore, the cytotoxicity of the prepared ZnO nanoparticles on mice cells is assessed, revealing lower toxicity for green-synthesized ZnO compared to chemically synthesized ZnO. Payne effect analysis on the composites demonstrates improved polymer-filler interaction and mechanical properties for the green-synthesized ZnO-loaded composites. Notably, the incorporation of green-synthesized ZnO leads to significant enhancements in tensile strength due to its higher surface area. It achieves desirable magic triangle tire properties, including low rolling resistance, high wet traction, and high abrasion resistance. These findings highlight the promising potential of green ZnO as an environmentally friendly alternative to chemical ZnO in rubber compounding.

Keywords: *activator, sustainability, tyre, Payne effect, zinc oxide*

1. Introduction

In recent years, there has been a significant increase in the demand for eco-friendly additives in rubber compounding [1]. Conventional rubber additives often harm the environment, prompting the search for sustainable alternatives. These sustainable additives, characterized by reduced toxicity and enhanced environmental friendliness, aim to improve rubber properties while maintaining optimal performance. There have been studies on using bio-based fillers, accelerators, and plasticizers in rubber compounds [2–5]. By adopting these advancements, the rubber industry can move towards a more sustainable and durable future [6]. However, the application of sustainable activators in rubber compounding remains limited and underexplored.

Zinc oxide (ZnO) is termed the best activator in rubber compounding due to its rapid cure kinetics and formation of short sulfide linkages, improving rubber products' overall performance [7, 8]. Recent studies have focused on developing sustainable ZnO nanoparticles using biological substances instead of traditional chemical and physical methods. Nanoparticles produced through green synthesis are cost-effective, non-toxic, and biodegradable [9, 10]. Investigating the use of these green-synthesized ZnO in rubber compounding is essential, as the rubber industry consumes 50–60% of the global annual production of ZnO [11]. Utilizing natural resources such as leaves, roots, floral extracts, and microorganisms (*e.g.*, bacteria, fungi, algae) in this eco-friendly synthesis approach reduces the use of harmful

---

[*]Corresponding author, e-mail: knaskar@rtc.iitkgp.ac.in

compounds [12, 13]. The bottom-up approach allows for the biogenic-like synthesis of nanoparticles by assembling atoms into nuclei and enabling their growth into nanoparticles, eliminating the need for external reducing, stabilizing, and capping agents [14]. Different parts of the plant, such as seeds, fruits, bark, stems, roots, shoots, leaves, and flowers, contribute biomass and secondary metabolites, including flavonoids, alkaloids, saponins, steroids, and tannins and these compounds act as both reducing agents and stabilizers [15, 16].

Citrus is a major fruit crop globally, with an estimated annual production of around 100 million metric tonnes. The peels of orange make up approximately 50 to 65 percent of its weight and are typically discarded as a by-product. The citrus peel contains diverse natural antioxidants, making it a valuable resource for the green synthesis of nanoparticles. Studies have shown that ZnO nanoparticles synthesized using *Citrus sinensis* peel extract (SNP) have similar crystal structures to commercial ZnO nanoparticles (CNP) but exhibit higher crystallinity and larger particle sizes. Citrus fruits contain significant quantities of ascorbic acid, a reducing agent or antioxidant. Comparing the ascorbic acid amount in citrus fruits like orange, pomegranate, and sweet lime, it was discovered that sweet lime peels contained significantly higher levels of ascorbic acid, 14.39±0.78 mg/ml. In contrast, lemon peels contain 3.05±1.19 mg/ml, and orange peel contains 3.87±0.77 mg/ml. Pomegranate peel contains 3.44±0.16 mg/ml.

In this study, we have selected sweet lime peel as a source for the synthesis of ZnO. Besides green synthesis, chemical precipitation methods were also employed to prepare the ZnO in this study. It has been previously explored that the synthesis method employed significantly impacts the particle size and surface area of ZnO nanoparticles [17, 18]. Its particle size and surface area influence the mechanical and dynamic properties of rubber compounds [19–21]. It has been demonstrated that smaller particle sizes and higher surface area enhance dispersion, cure kinetics, and overall performance of rubber compounds [22–24]. Research has shown that the presence of highly reactive Zn ions in the higher surface area ZnO facilitates the formation of a protective outer layer on the silica surface in the silica-filled compound by forming Si–O–Zn bond formation. This protective layer reduces filler-filler interactions, thus enhancing polymer-filler interactions in silica-filled rubber compounds [25–27]. This research also aims to elucidate the effect of synthesized green and chemical ZnO on the silica filler and its effects on the polymer-filler interaction.

The novelty and primary objective of this study lie in the use of these green-synthesized ZnO from sweet lime peel as an activator in rubber compounding, a topic not yet thoroughly explored. The study compares the structural and thermal properties of green-synthesized ZnO with chemically synthesized ZnO. It explores the cytotoxicity of green- and chemical-synthesized ZnO in mice cells. The study primarily examines the effects of these synthesized ZnO on rubber compounds in terms of rheological properties, mechanical properties, thermal properties, and the ‘magic triangle’ attributes of tires, such as rolling resistance, traction, and wear resistance. This study also investigates how the synthesis method affects the surface characteristics of ZnO, its interaction with silica filler, and its effects on the polymer-filler interaction.

2. Materials

Zinc nitrate hexahydrate, the zinc precursor, was acquired from Loba Chemie in India. Pellets of sodium hydroxide (NaOH) were obtained from Merck India. The juice store in the local market near IIT Kharagpur, West Bengal, India, supplied the sweet lime peels. Green ZnO is referred to as G ZnO, and chemically synthesized ZnO is denoted as C_H ZnO throughout the text. The SVR 3L natural rubber was obtained from Kurian Abraham Pvt. Ltd. in India. Jain Chemicals Ltd. in India supplied the coupling agent triethoxysilyl propyl tetrasulfide (TESPT), highly dispersible silica (HDS) (Solvay, India), stearic acid (Nocil, India), hydroquinone (HQ) (Nocil, India), *n*-cyclobenzyl-2-benzothiazole sulfenamide (CBS) (Nocil, India), and sulfur.

2.1. Synthesis of green and chemical ZnO

2.1.1. Extract preparation from sweet lime peels

The sweet lime peels were collected from a local juice shop at IIT Kharagpur, West Bengal, India. After cleaning with tap and distilled water, they were dried at 60 °C for 24 h. The peels were dried and pulverized into powder and mixed in a 1:50 ratio with distilled water. After stirring for 3 h, the mixture was allowed to macerate and kept in a water bath at 80 °C for 2 h at 300 rpm. The mixtures were filtered with Whatman filter paper, and the extract was then kept at 4 °C for further use.

2.1.2. Synthesis of green ZnO using sweet lime peel extract

ZnO was synthesized from sweet lime using a previously described method [28] with appropriate reaction conditions and reducing agent modifications. 2 g of zinc nitrate hexahydrate was combined with 42.5 ml of sweet lime peel extract in a beaker. The solutions were agitated for 60 min at 25 °C, then transferred to a water bath at 60 °C for another 60 min. Afterward, the mixtures were dried at 150 °C until they reached a thick, caramel-like consistency. Finally, the resulting material was calcinated in a muffle furnace at 500 °C for 3 h (Figure 1).

2.1.3. Synthesis of ZnO using chemical precipitation method

A 500 ml solution of zinc nitrate hexahydrate at a concentration of 20 mM was prepared in distilled water. Concurrently, a 20 mM NaOH solution was prepared and added to the round bottom flask. The mixture was stirred at 300 rpm for 2 h and refluxed at 60 °C (Figure 2). The powder was dried in a hot air oven at 80 °C for 24 h after centrifuged at 5000 rpm for 10 min. The chemical synthesis of ZnO was conducted using a preparation method derived from a previous research article, with minor adjustments to the reaction conditions [29].

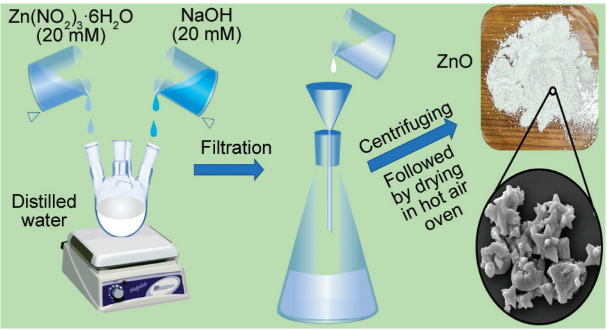

Figure 2. Chemical synthesis of ZnO using the precipitation method.

2.2. Characterization of ZnO nanoparticles

The crystallinity of the synthesized chemical and green ZnO was analyzed using a Brucker high-resolution X-ray diffractometer (HR-XRD) (Migdal Haemek, Israel). Crystallite sizes were calculated utilizing Bragg's equation. PerkinElmer (UK) Ltd., Buckinghamshire, United Kingdom was employed to observe the functional groups present in the synthesized ZnO. The absorption peaks (λ_{max}) of the ZnO nanoparticles were determined by analyzing the UV-Visible spectrum (200–700 nm) with the UV-Vis spectrophotometer (Shimadzu, Japan). Scanning

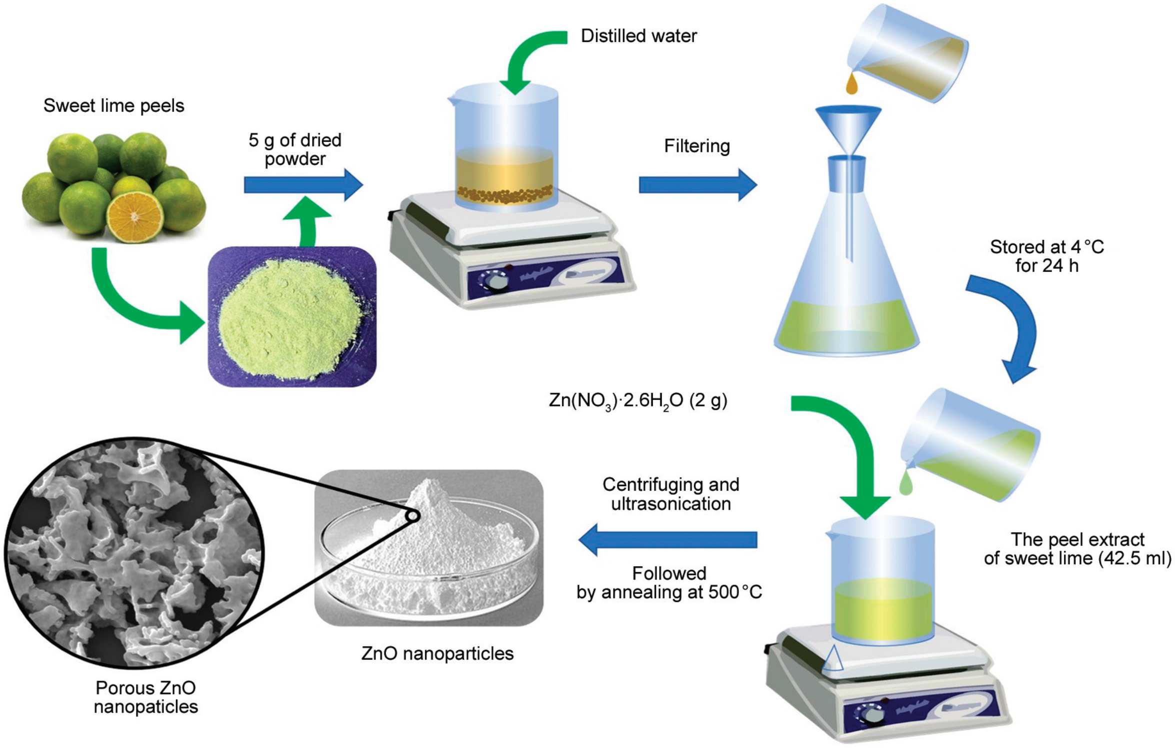

Figure 1. Green synthesis of ZnO from sweet lime peel extract.

electron microscopy (MERLIN-ZEISS EVO 60, Germany) evaluated the nanostructure, size distribution, and agglomeration of the obtained nanoparticles. The use of Scanning Electron Microscopy (SEM)-Energy Dispersive X-ray Analysis (EDX) techniques allowed for elemental analysis and, subsequently, the calculation of elemental proportions. The N_2 adsorption-desorption measurements were employed to identify the Brunauer-Emmett-Teller (BET) surface area [m^2/g] of the chemically synthesized and green synthesized ZnO. This was achieved using the Nova Station A instrument. The X-ray photoelectron spectroscopy (XPS) was employed to analyze the surface chemical composition of the ZnO nanoparticles in their as-prepared state. The analysis used a PHI 5000 VERSA PROBE III. model X-ray photoelectron spectrometer (Physical Electronics, Inc. (PHI), Minnesota, USA). The measurements were conducted on drop-casted ZnO powder, which was affixed to the sample holder using carbon tape. The X-ray photoelectron spectroscopy (XPS) was conducted in an ultrahigh vacuum environment with a base pressure of $5\cdot10^{-10}$ mbar at room temperature. The XPS measurements were performed using an Al K_α source gun. To mitigate the influence of charging effects, the X-ray photoelectron spectroscopy (XPS) spectra were calibrated by establishing a constant value for the binding energy (BE) of the C 1s peak originating from atmospheric contamination, which was set at 284.8 eV.

2.2.1. Cytotoxicity of synthesized ZnO nanoparticles: Cell culture and MTT assay

The HT-22 hippocampal cells obtained from Dr. Dave Schubert at the Salk Institute in the USA were cultivated in a complete Dulbecco's Modified Eagle Medium (DMEM) medium. The culture medium utilized in this study consisted of heat-inactivated fetal bovine serum (FBS) at 10% obtained from Invitrogen (Waltham, USA), along with penicillin/streptomycin at 1% concentration. The cells were cultured at 37 °C in an environment with 5% carbon dioxide (CO_2). The cells were distributed in a 96 well tissue culture plate at a density below the confluence. Following 24 h, the subjects were subjected to a range of concentrations (1, 5, 10, 25 µg/ml) of ZnO, which had been dissolved in double-distilled water. These particular doses were selected based on prior research. Following a 12 h exposure period, the cells were washed using 100 µl of phosphate-buffered saline (PBS). Then, 100 µl of Thiazolyl Blue Tetrazolium Bromide (MTT) (33611, Sisco research laboratories Pvt.Ltd (SRL)) in phosphate-buffered saline (PBS) at a concentration of 2 mg/ml was introduced to each well and subjected to incubation under identical conditions for 3 h. After incubation, the MTT solution was completely aspirated and subsequently substituted with 100% dimethyl sulfoxide (DMSO). The optical density measurement at a

Table 1. Rubber composite recipes.

Ingredients[a] [phr]	G1-NC	G3-NC	G5-NC	C1-NC	C3-NC	C5-NC
Natural rubber	100	100	100	100	100	100
G ZnO[b]	1	3	5	–	–	–
C_H ZnO[c]	–	–	–	1	3	5
Stearic acid	2	2	2	2	2	2
HDS[d]	50	50	50	50	50	50
TESPT[e]	5	5	5	5	5	5
TDQ[f]	1	1	1	1	1	1
Wax	2	2	2	2	2	2
CBS[g]	1.25	1.25	1.25	1.25	1.25	1.25
S[h]	2.5	2.5	2.5	2.5	2.5	2.5

[a] parts per hundred rubber,
[b] green synthesized zinc oxide,
[c] chemically synthesized zinc oxide,
[d] highly dispersible silica,
[e] tetraethyl thiuram disulfide,
[f] trimethyl-dihydroquinolines,
[g] cyclobenzyl sulfenamide,
[h] sulfur.

wavelength of 595 nm was conducted, and subsequent analysis of the results was performed using GraphPad software.

2.3. Composite preparation

The composite was developed based on the formulation provided in Table 1. The composite's preparation involved a two-stage mixing process, comprising the creation of a masterbatch and a final batch.

The masterbatch, which included all additives except curatives, was meticulously prepared using a Brabender plasti-corder internal mixer (Germany). Subsequently, the final batch was formed by introducing the curatives in two roll mills (Santhosh Rubber Machinery Pvt. Ltd, India). During the masterbatch blending phase, the temperature was maintained at 140 °C. At the outset of the mixing process, the rubber and activators were introduced at 30 rpm. Following the inclusion of the remaining compounding ingredients, the mixing speed was elevated to 60 rpm, and the overall mixing duration was 4.5 min. These compositions included 1, 3, and 5 phr of green or chemically synthesized ZnO. They were denoted as G1-NC, G3-NC, G5-NC, C1-NC, C3-NC, and C5-NC.

2.4. Characterization of natural rubber composites with C_H ZnO and G ZnO as activator

2.4.1. Cure characteristics of composites

The cure characteristics of the natural rubber composites were observed by placing them in a moving die rheometer (Monsanto Rheometer (MDR 2000), Akron, USA) at a temperature of 150 °C for 30 min with an oscillation angle of 3°.

2.4.2. Crosslink density from swelling study

The crosslink density of a sample measuring 10×10×2 mm was determined by swelling experiments in toluene for 72 h at room temperature. The volume fraction of the polymer in the swollen network (V_r) was determined using the provided Equation (1) [30, 31]:

$$V_r = \frac{\frac{D - fH}{\rho_r}}{\frac{D - fH}{\rho_r} + \frac{A_0}{\rho_S}} \tag{1}$$

where D represents deswollen weight, H is the test specimen weight, f is the weight fraction of insoluble components, and ρ_r and ρ_s are the polymer and solvent density. A_0 is the weight of the absorbed solvent.

The apparent crosslink density was determined by using the modified Flory–Rehner equation (Equation (2)) [32, 33]:

$$-\left[\ln(1 - V_r) + V_r + \chi V_r^2\right] = \frac{\rho_r V_m \left(\sqrt[3]{V_r} - 0.5V_r\right)}{2M_c} \tag{2}$$

where V_m denotes the molecular volume of the toluene which is 106.3 ml/mol. The Flory-Huggins interaction parameter, denoted as χ, is 0.36 for the NR-toluene system [34]. The M_c gives the cross-link density in mol/cm^3.

2.4.3. Thermal response of rubber compounds from thermogravimetric analysis

Thermogravimetric analysis (TGA) is used to determine the thermal stability of the silica-filled rubber compounds using a Shimadzu TGA 50 (Shimadzu, Japan) device in a nitrogen environment to prevent oxidation effects. The mixtures are weighed to about 8 to 10 g and then placed in a graphite crucible. They are then heated from 30 to 800 °C at 10 °C/min.

2.4.4. Strain sweep analysis from rubber process analyzer

The prepared rubber blends viscoelastic properties were measured in a Rubber Process Analyzer RPA 2000, Alpha Technologies, Hudson, Ohio. At a constant temperature of 100 °C for the strain sweep study. The strain was adjusted from 0.05 to 100% while maintaining a 0.33 Hz frequency. Every parameter was calculated as a function of strain.

2.4.5. Mechanical properties

The composite tensile strength, break elongation, and modulus were measured in ambient circumstances using a Hioks-Hounsfield universal testing machine (Test Equipment Ltd, Surrey, England) with a 500 mm/min crosshead speed. The specimens were cut from the molded sheet according to ASTM D412 die C. The hardness is measured on a Shore A scale using a durometer hardness tester.

2.4.6. Statistical analysis

The significance of the type and amount of ZnO used in the study on the mechanical properties of rubber compounds (C1-NC, C3-NC, C5-NC, G1-NC, G3-NC, and G5-NC) was verified using ANOVA statistical tools. A statistical ANOVA single-parameter test was conducted with a p-value of ≤ 0.05. The ANOVA single-parameter test analyzed the tensile strength, elongation at break, modulus, hardness, and tear strength studies.

2.4.7. Aging study

To comply with ASTM D573 standards, accelerated aging was conducted using a forced air circulating oven (Blue M Electric, model no F0 712, Blue Island, Illinois, USA). The aging process was performed at 70 °C for one week. After aging, the mechanical properties of the specimens were evaluated following a 40 h conditioning period at 23 °C and 50% relative humidity to ensure thermal equilibrium. Aged samples' mechanical properties were compared to unaged samples according to the test mentioned in Section 2.4.5.

2.4.8. Dynamic mechanical analysis and abrasion resistance

The dynamic mechanical characteristics of the mixes were assessed in tension mode using an Eplexor 2000 instrument from Gabo Qualimeter (NETZSCH-Geratebau GmbH, Selb, Germany). The sample size was 35×10×2 mm, and temperature sweeps from –80 to 80 °C with 0.5% dynamic strain and 1% static strain were carried out using heating rates of 2 K/min at a test frequency of 10 Hz. Abrasion resistance was performed with a DIN abrader as per DIN ISO 4649.

3. Results and discussion

3.1. Structural characterization of ZnO nanoparticles

The formation of ZnO particles from the chemical and green synthesis has been confirmed by X-ray diffraction analysis. Figure 3a gives the diffraction pattern of chemically synthesized ZnO, denoted as C_H ZnO, and ZnO synthesized from green sources, denoted as G ZnO. The diffraction peaks at 31.81, 34.47, 36.26, 47.63, 56.63, 62.88° and corresponding to 68.00° to lattice planes of (110), (002), (101), (102), (110), (103) and (112) respectively (JCPDS: 36-1451) [35] it confirms the both synthesized green and chemical ZnO were having hexagonal wurtzite crystal structure of ZnO crystals. Crystallite size was calculated using the Scherrer equation given below. The obtained crystallite size was 21.17 nm for C_H ZnO and 7.83 nm for G ZnO (Equation (3)):

$$D = \frac{K\lambda}{\beta\cos\theta} \tag{3}$$

In the Scherrer equation D – crystallite size, K – Scherrer constant (value = 0.94), λ – X-ray wavelength, β – the reflection width (2θ), θ – the Bragg angle. In Figure 3b, FTIR peaks ranging from 4000 to 400 were observed, indicating the presence of ZnO vibrations in the ZnO nanoparticles [36, 37]. The stretching mode of ZnO was observed at a wavenumber of 489 cm^{-1} for C_H ZnO and 557 cm^{-1} for G ZnO. The presence of peaks at 773 and 853 cm^{-1} indicates the coordination of Zn^{2+} in the tetrahedral position [37]. The peak in the wavenumber range of 1300–1500 cm^{-1} was attributed to the stretching vibration of the C–O bond in both C_H ZnO and G ZnO [38].

The UV-visible absorption spectra of ZnO nanoparticles are depicted in Figure 3c. These nanoparticles were synthesized using green and chemical methods. The ZnO nanoparticles demonstrate a wider absorption peak ranging from 330 to 380 nm. The findings closely align with the outcomes reported by other investigators [39, 40]. UV-visible spectroscopy is a highly useful technique for analyzing nanoparticle dimensions and morphology. A peak absorption at

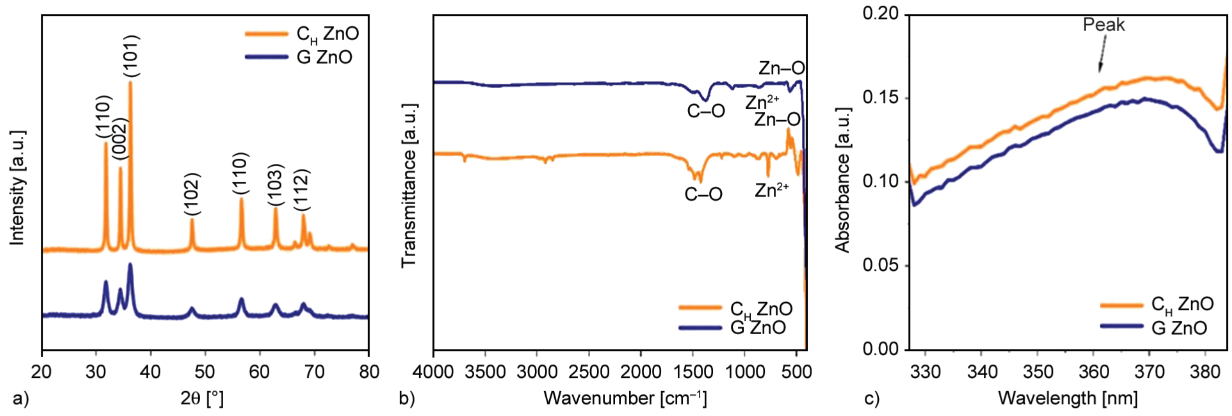

Figure 3. a) XRD, b) FTIR, c) UV absorption spectra of C_H ZnO and G ZnO.

shorter wavelengths suggests a reduction in particle size [29]. In this case, the absorption peak wavelengths for G ZnO were slightly lower than those for C_H ZnO, thus confirming that the crystallite size determined through XRD analysis aligned with the UV absorption analysis.

3.2. Morphology and BET surface area of synthesized ZnO

Reaction temperature, pH value of the solution, and precursor concentration depend on the morphology of the ZnO formed. Figure 4 depicts SEM images of chemically and green-synthesized ZnO. A flower-like structure with petals approximately 1 µm in size is observed in the C_H ZnO, while the G ZnO exhibits a porous structure. Pore size and flower petal size were calculated using Image J software. The BET surface area was determined through the nitrogen absorption method, revealing that C_H ZnO possesses a surface area of 13.46 m^2/g, and G ZnO exhibits a significantly greater surface area of 44.55 m^2/g, approximately 2.3 times higher than that of C_H ZnO.

The ZnO nuclei form a flower-shaped structure as the concentration of precursor increases. Here, we used a 2 mM precursor, resulting in ZnO's flower morphology. As previously reported in the literature, the anisotropic growth of ZnO is advantageous when the pH value of the medium exceeds 7. In this case, NaOH was employed to achieve a basic pH in the medium. In the present study, we used water medium as a solvent to aid in the formation of flower-like nanostructures of ZnO by adjusting the homogenization of the reactants in the reaction medium, the amount of individual nucleus formation, and the amalgamation and direction preference of the growing nucleus. An annealing temperature of 500 °C was applied to green ZnO, forming a porous ZnO structure.

3.3. Zeta potential and EDX analysis of synthesized ZnO

Nanoparticles (NPs) have significant surface area relative to their volume, with exposed bonds and charged groups. When placed in water, NPs undergo surface ionization, drawing in ions and building up a surface charge. This difference in charge generates an electric potential between NPs and the surrounding liquid, quantified as zeta potential in electrokinetic studies. The ζ-potential is a crucial parameter for evaluating the colloidal stability of said particles and offers valuable information regarding their surface charge. The surface charge of both chemically synthesized and environmentally friendly synthesized ZnO particles was examined through dynamic light scattering (DLS). The investigation found that the ζ-potential of C_H ZnO nanoparticles in distilled water (DW) was recorded at –39.8 mV, indicating a strong anionic charge. The ζ-potential of G ZnO nanoparticles in distilled water (DW) was recorded at –25.6 mV. This measurement confirms and substantiates the ability of G ZnO-NPs to disperse effectively. The negative surface charge results from the binding interaction between the extract compounds and the nanoparticles, which imparts stability to the zinc oxide nanoparticles and reduces their tendency to aggregate.

3.4. XPS analysis of synthesized ZnO

Figure 5a shows the broad scan of the XPS spectrum. Figure 5b displays the Zn 2p spectrum of C_H ZnO and G ZnO particles. In this spectrum, we observe two distinctive peaks: Zn $2p_{3/2}$ at 1021.7 eV and Zn $2p_{1/2}$ at 1044.7 eV. These two peaks are separated by a gap of 23.1 eV, indicating the existence of Zn^{2+} within the Zn component [41]. A subtle difference in the binding energies of the Zn 2p constituents can be discerned in Figure 3b. This observed phenomenon

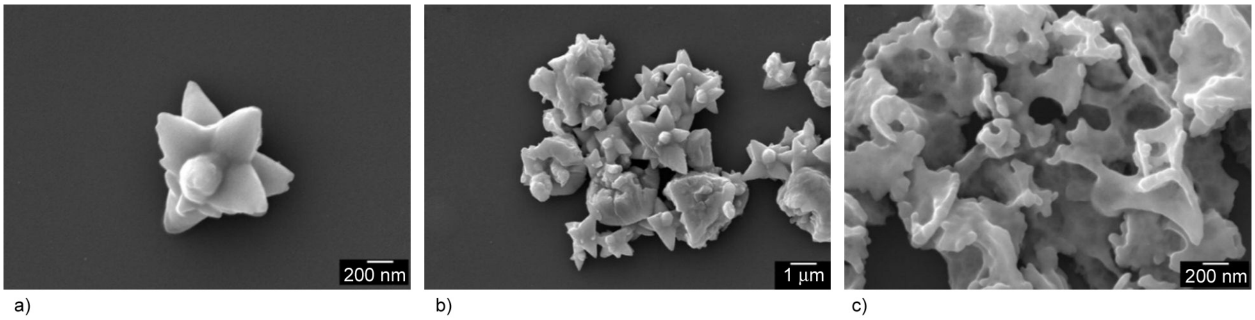

Figure 4. SEM images of a) C_H ZnO, b) its aggregate structure of C_H ZnO, c) the porous structure of G ZnO.

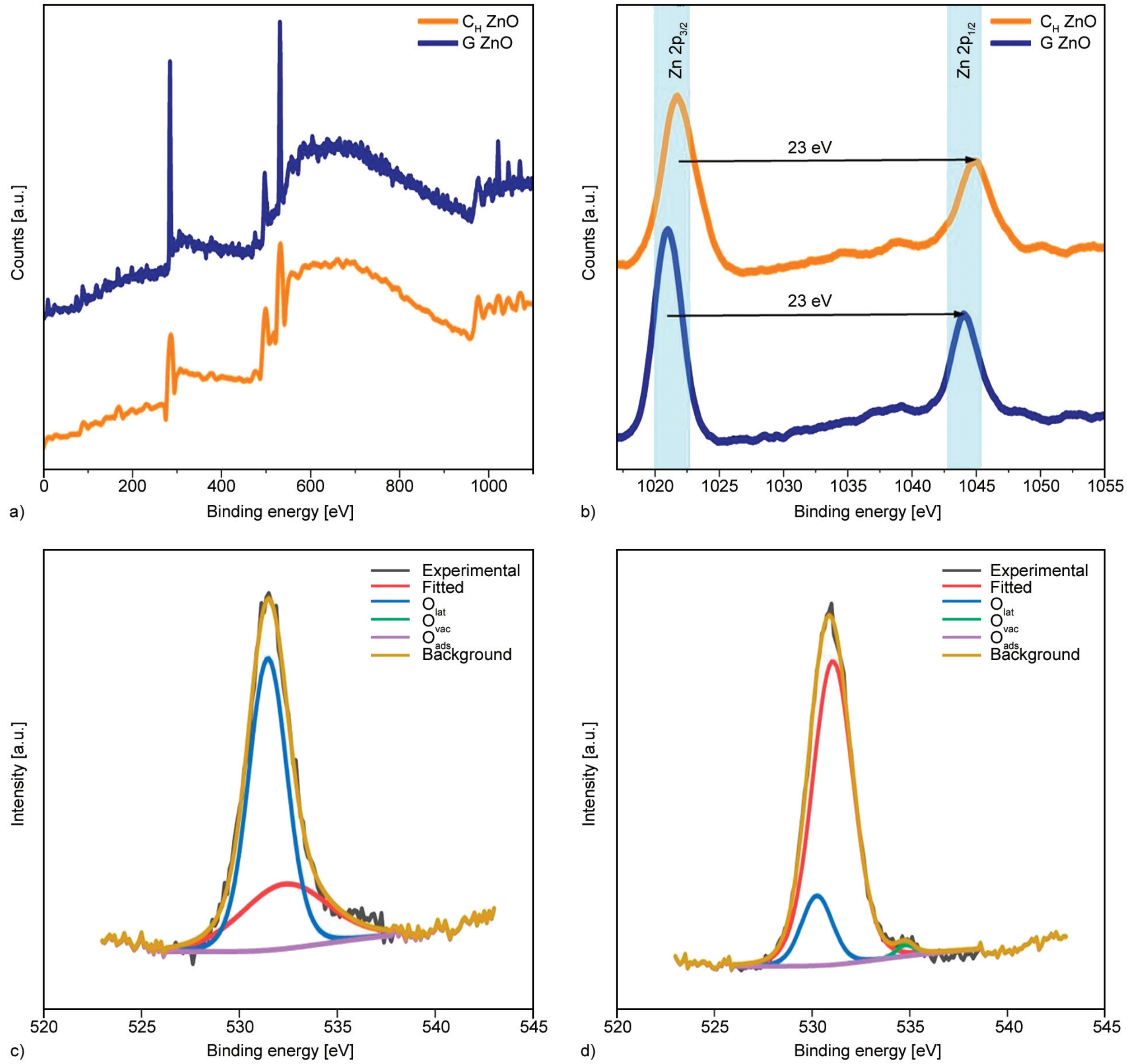

Figure 5. XPS analysis of a) C_H ZnO and G ZnO full spectrum, b) Zn spectrum, c) O 1s XPS spectra for the C_H ZnO and d) G ZnO. Where O_{lat} is lattice oxygen, O_{vac} is vacancy oxygen, O_{ads} is adsorbed oxygen.

is probably a result of the varied surface morphologies displayed by ZnO nanostructures [42].

3.5. Cytotoxicity of synthesized ZnO nanoparticles

Investigated the cytotoxicity of C_H ZnO and G ZnO at 1, 5, 10, and 25 µg/ml doses on HT 22 hippocampal cells. The MTT assay measures mitochondrial activity by turning MTT into formazan crystals through live cells. This assay commonly evaluates different medicines' *in vitro* cytotoxic effects on cell lines. Therefore, mitochondrial activity is associated with the percentage of viable cells among the total cell population. In the experiment, cells were examined by MTT assay to check the cytotoxicity of C_H ZnO and G ZnO. The HT-22 cells were treated at 1, 5, 10, and 25 µg/ml dose for 12 h. The percentage of cell viability index [%] was calculated using the Equation (4) [43]:

$$\text{Cell viability index} = \frac{\text{OD test sample} - \text{OD negative control}}{\text{OD positive control} - \text{OD negative control}} \cdot 100 \tag{4}$$

where OD is the optical density.

Obtained cell viability of nano, functionalized, active, and conventional ZnO is shown in Figure 6. MTT assay shows cell viability was decreasing with the increasing ZnO concentration. The G ZnO had more cell viability than C_H ZnO, showing that

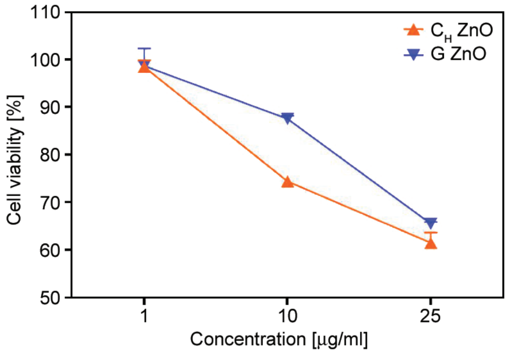

Figure 6. Cytotoxicity of C_H ZnO and G ZnO particles in HT.22 hippocampal cells.

G ZnO is less toxic than C_H ZnO and makes a more sustainable alternative to C_H ZnO.

3.6. Cure characteristics of rubber composites

The cure characteristics were performed in the Moving Die Rheometer to get insight into the influence of C_H ZnO and G ZnO as activators in the natural rubber matrix (MDR200). From the the curve, the maximum torque (M_H), minimum torque (M_L), scorch time, optimum cure time, and cure rate index are obtained. The obtained parameters are listed in Table 2.

The minimum torque is connected to the viscosity of the rubber compounds, the maximum torque is indicative of the stiffness of the vulcanizate during curing, and the torque difference reflects the extent of crosslinking within the material [44]. The primary variables affecting the crosslink density of the vulcanized system are the maximum torque (M_H) and delta torque ($M_H - M_L$), as shown by the rheometer curve in Figure 7.

Table 2. Cure characteristics of natural rubber vulcanizates.

Entry	M_L [dN·m]	M_H [dN·m]	$M_H - M_L$ [dN·m]	Ts [min]	Tc_{90} [min]	CRI [min^{-1}]
C1-NC	4.75	22.89	18.14	4.28	10.18	16.97
C3-NC	5.83	26.00	20.17	6.11	22.58	06.07
C5-NC	6.36	30.29	23.93	6.41	23.23	05.95
G1-NC	5.68	24.40	18.72	4.71	10.85	16.29
G3-NC	5.34	27.10	21.76	6.57	21.93	06.51
G5-NC	5.81	27.76	21.95	7.06	22.91	06.31

The resistance to deformation in an elastomer is directly related to the density of network-supporting polymer chains. A greater number of junctures leads to an increased presence of supporting chains, resulting in an anticipated rise in M_H at elevated values of network chain density [45].

It was observed that with the increasing addition of both chemical and green ZnO, the M_H value increased, and the crosslink density increased correspondingly. However, the M_H, $M_H - M_L$, and crosslink density values of silica composites filled with green ZnO activator were high, and this could be due to the lower crystallite size of G ZnO obtained from the XRD study. These results were in line with the study observed by the other authors [46].

Interestingly, the cure time (Tc_{90}), t_{s2} was increased with the increase of G ZnO and C_H ZnO amount accompanied by a decrease in cure rate index (CRI). This phenomenon is attributed to the extended time needed for chelate complex formation with a higher concentration of Zn ions [47]. G ZnO-filled

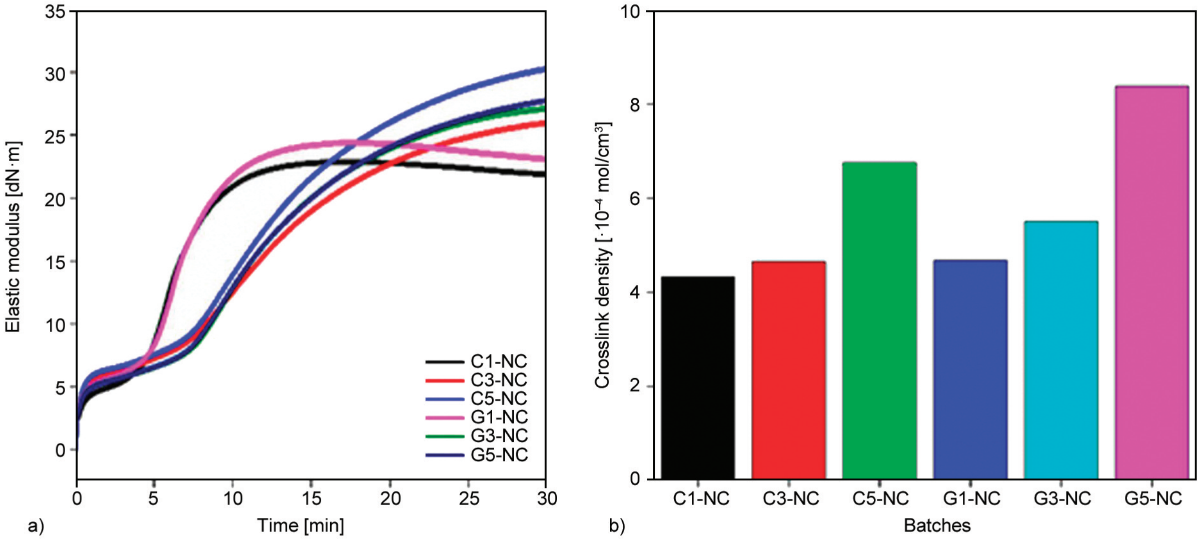

Figure 7. a) Cure characteristics composites with C_H ZnO and G ZnO, b) crosslink density of composites with C_H ZnO and G ZnO.

composites, with their greater effective surface area, displayed a notably slower cure rate compared to C_H ZnO-filled composites. The enhancement in the maximum torque (M_H) value, resulting from increased ZnO content at 1, 3, and 5 phr, is explained by the formation of chelate compounds between Zn^{2+} ions in ZnO and the rubber-Sxy-accelerator. This interaction accelerates vulcanization during the initial stage, leading to a higher vulcanization rate than the free accelerator. Additionally, the increase in scorch time (Ts_2) and Tc_{90} is linked to the prolonged decomposition time of ZnO during the rubber-Sxy-accelerator combination process, attributable to the elevated Zn^{2+} content. The cure rate is influenced by the availability of zinc ions in chelates, with G ZnO containing more zinc ions due to its higher surface area than C_H ZnO [48–50].

3.7. TGA analysis of C_H ZnO, G ZnO, and composites

Figure 8a demonstrates the thermal degradation profile of C_H ZnO and G ZnO. Results demonstrated that the G ZnO exhibited notable thermal stability.
The observed weight reduction, amounting to approximately 4.21% of the initial weight, can be attributed to a gradual process of weight loss occurring within the temperature range of room temperature to 800 °C. This phenomenon is most likely caused by the evaporation of moisture content and the degradation of organic substances in the samples. On the other hand, 14.60% weight loss was observed in C_H ZnO.

Where Figure 8b and c show the degradation profile of composites filled with C_H ZnO and G ZnO, the thermal stability of composites with G ZnO was higher than C_H ZnO-loaded composites, and with 1 phr loading, the thermal stability was lower. The maximum temperature (T_{max}) was observed at 386.72, 387.35, and 389.76 °C for C1-NC, C3-NC and C5-NC, respectively. Whereas the T_{max} was 387.35, 387.73, 389.38°C for G1-NC, G3-NC and G5-NC. With the higher addition of ZnO, the thermal stability increased due to ZnO increasing the composite's heat resistance.

3.8. Payne effect of rubber composites

As per the Payne effect theory, the relationship between low deformations pertains to the interactions between rubber and filler materials, while high deformations are mainly attributed to interactions among the filler particles themselves. The greater the ΔG ($\Delta G = (G'_0 - G'_\infty)$) value, the more pronounced the Payne effect becomes, indicating higher filler-filler interactions and increased clusters within the elastomeric matrix. A low Payne effect shows good polymer-filler interaction. Here, with the higher addition of both types of ZnO, the Payne effect was decreased, as seen in Figure 9. In the presence of G ZnO, the composites exhibit a lower Payne effect than the C_H ZnO-loaded composites. In our previous study, it has been shown that in silica-filled compounds, the presence of highly reactive Zn^{2+} ions promptly interacted with the silica surface to create the covalent link Si–O–Zn. This layer protected the

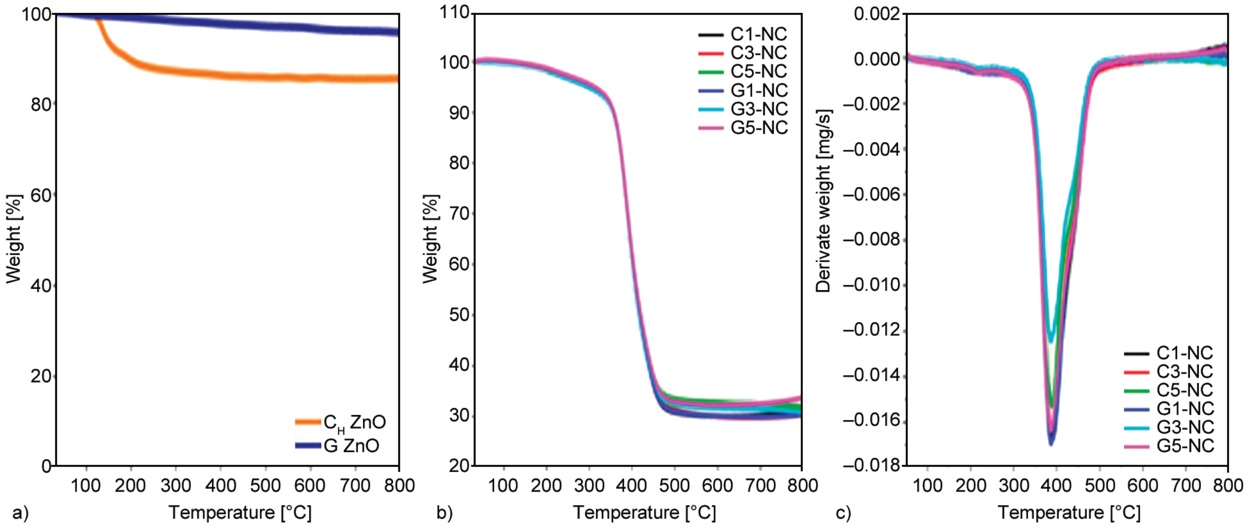

Figure 8. TGA analysis of a) C_H ZnO and G ZnO, b) rubber compounds filled with C_H ZnO and G ZnO, c) DTG curve of compounds filled with C_H ZnO and G ZnO.

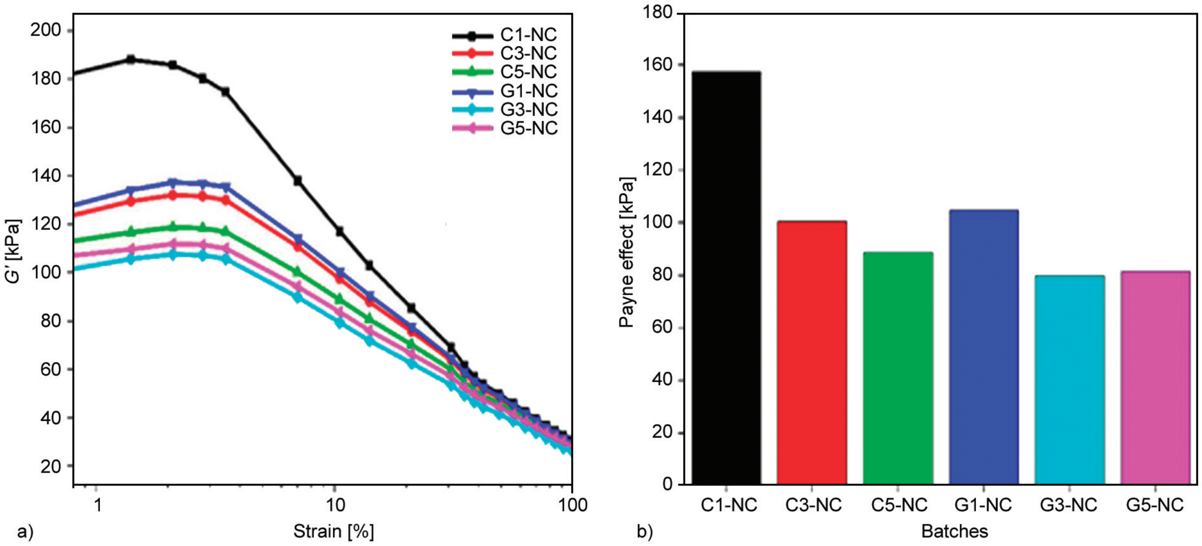

Figure 9. a) Strain sweep curve of silica composites with C_H ZnO and G ZnO, b) Payne effect in composites.

silica particles and reduced the filler's aggregation in the matrix [25, 27, 51].

With a high surface area, the no of reactive Zn^{2+} ions will be higher on the surface of the ZnO particles. Here, the surface area of C_H ZnO was 13.46 m^2/g, whereas G ZnO had a surface area of 44.55 m^2/g; this enables the higher Zn^{2+} ions on the surface of G ZnO, and this tends to form a protective layer on the surface of silica particles and reduces the filler-filler interaction and improves the polymer -filler interaction that has been elucidated from the Payne effect analysis as shown in Figure 9.

The number of Zn^{2+} ions increased with the amount of ZnO loading. Thereby, at higher loading of ZnO, the amount of Zn^{2+} ions was increased, and the Payne effect was lower at C5-NC, G3-NC, and G5-NC. The high surface area of ZnO can lead to agglomeration, which also results in the same Payne effect of G5-NC and G3-NC. The morphological analysis of rubber compounds was consistent with the observed Payne effect result, and a detailed SEM analysis was provided in the supporting information (S1).

3.9. Mechanical properties of rubber composites

The mechanical properties of natural rubber composites loaded with G ZnO and C_H ZnO are listed in Table 3.

The reflectance of the Payne effect was shown in the mechanical properties of composites loaded with 1,3 and 5 phr of G ZnO or C_H ZnO and designated as G1-NC, G3-NC, and G5-NC for G ZnO-loaded compounds and C1-NC, C3-NC, and C5-NC for C_H ZnO-loaded batches. Tensile strength, elongation at break, modulus, tear strength, and hardness were increasing with the addition of ZnO. The tensile strength of C3-NC was 19.6% higher than the C1-NC compound. An enhancement of 3.5% in tensile strength was observed in G3-NC filled with G ZnO compared to G1-NC. Meanwhile, in 5 phr loading, both C_H ZnO- and G ZnO-loaded compounds exhibited high tensile strength values and were highest in compounds with G ZnO. From C3-NR and G3-NR, the increase in tensile strength observed was 200 and 64%, respectively, for C5-NR and G5-NR. The

Table 3. Mechanical properties of natural rubber vulcanizates.

Sample designation	Tensile strength [MPa]	Elongation at break [%]	Modulus at 300% [MPa]	Tear strength [N/mm]	Hardness [Shore A]
C1-NC	6.1±1.4	883±91	1.3±0.4	33.5±2.8	62±3
C3-NC	7.3±1.0	900±91	1.4±0.4	40.4±4.2	62±2
C5-NC	22.6±0.4	903±10	4.0±0.1	85.8±1.1	64±1
G1-NC	14.6±0.7	863±29	2.3±0.1	60.6±7.7	62±2
G3-NC	15.1±0.6	926±4	2.6±0.1	68.7±11.0	63±1
G5-NC	24.7±0.2	917±12	4.6±0.1	109.0±2.5	64±2

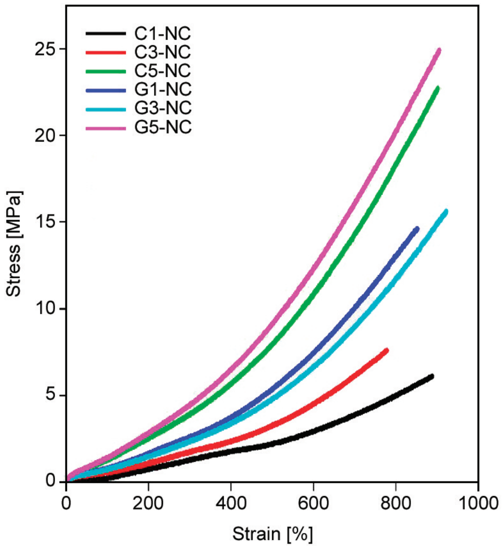

Figure 10. Stress-strain curve of silica composites with C_H ZnO and G ZnO.

G1-NC exhibited a 139% increase in tensile strength compared to C1-NC. The G3 NC and G5 NC showed increases of 106 and 9%, respectively, over C3-NC and C5-NC, and the stress-strain plot is shown in Figure 10.

Increased tear strength was also observed when the amount of ZnO increased in both C_H ZnO and G ZnO-loaded composites. The tear strength of C3-NC was enhanced by 20.5% compared to C1-NC, and C5-NC tear strength increased by 112.37% compared to C5-NC. In G ZnO-loaded ZnO, G3-NC exhibited a 13% improvement in tear strength compared to G1-NC. A 55.7% increase in tear strength was shown for G5-NC compared to G3-NC. The modulus was also reflected similarly to tear strength. It was increased by 7.69% from C1-NC to C3-NC, and from C3-NC to C5-NC, it was 185.71%. In G ZnO-loaded compounds, 13.04 % increase from G1-NC to G3-NC and 76.15% from G3-NC to G5-NC. The mechanical properties of G ZnO-loaded compounds improved due to the high crosslink density and high effective surface area of the G ZnO compared to C_H ZnO.

3.10. Statistical analysis using ANOVA single parameter

Using a statistical ANOVA single-parameter test, the significance of the type and quantity of ZnO used in the study was confirmed at a p-value of ≤0.05 regarding the mechanical properties of rubber compounds, such as C1-NC, C3-NC, C5-NC, G1-NC, G3-NC, and G5-NC. C1-NC, C3-NC, and C5-NC are chemical ZnO loaded in 1,3 and 5 phr, respectively. G1-NC, G3-NC, and G5-NC represent the 1, 3 and 5 phr of green ZnO in the rubber compounds. Table 4 presents a concise overview of the statistical analysis conducted using ANOVA. The ANOVA single-parameter test was employed to analyze studies on tensile strength, elongation at break, modulus, hardness, and tear strength and to determine the statistical significance between the groups. Among the five analyses conducted, the tensile strength, tear strength, and modulus exhibited significant variations based on the type of ZnO and the amount of ZnO loading in the rubber compounds. There were notable variations among the groups regarding tensile strength, with p-values of $1.58 \cdot 10^{-13}$ and $2.18 \cdot 10^{-8}$ for tear strength. Furthermore, a notable significance was observed in the modulus, with a value of $p = 3.62 \cdot 10^{-9}$. The p-value for elongation at break was 0.602109, while the p-value for hardness was 0.59756.

3.11. Aging properties of rubber composites

The thermal aging of natural rubber composites was conducted at 100 °C for 7 days. After the aging study, the changes in the crosslink density and mechanical properties were analyzed, as shown in Figure 11. The increase in overall crosslink density during the thermal aging process is attributed to the degradation of unstable polysulfide into mono and disulfide compounds [52]. The mechanical properties obtained were in correlation with the crosslink density observed. The tensile strength and modulus were increased, and the elongation at the break did not affect

Table 4. Summary of ANOVA analysis.

Mechanical properties	Source of variation	The sum of squares, SS	Degree of freedom, df	Mean square, MS	*f*-value	*p*-value
Tensile strength	Between the groups	836.344	5	167.269	507.507	$1.58 \cdot 10^{-13}$
Elongation at break	Between the groups	12173.400	5	2434.681	0.749	0.602
Modulus	Between the groups	27.406	5	5.481	92.904	$3.62 \cdot 10^{-9}$
Tear strength	Between the groups	11882.940	5	2376.587	68.139	$2.18 \cdot 10^{-8}$
Hardness	Between the groups	14.500	5	2.900	0.756	0.597

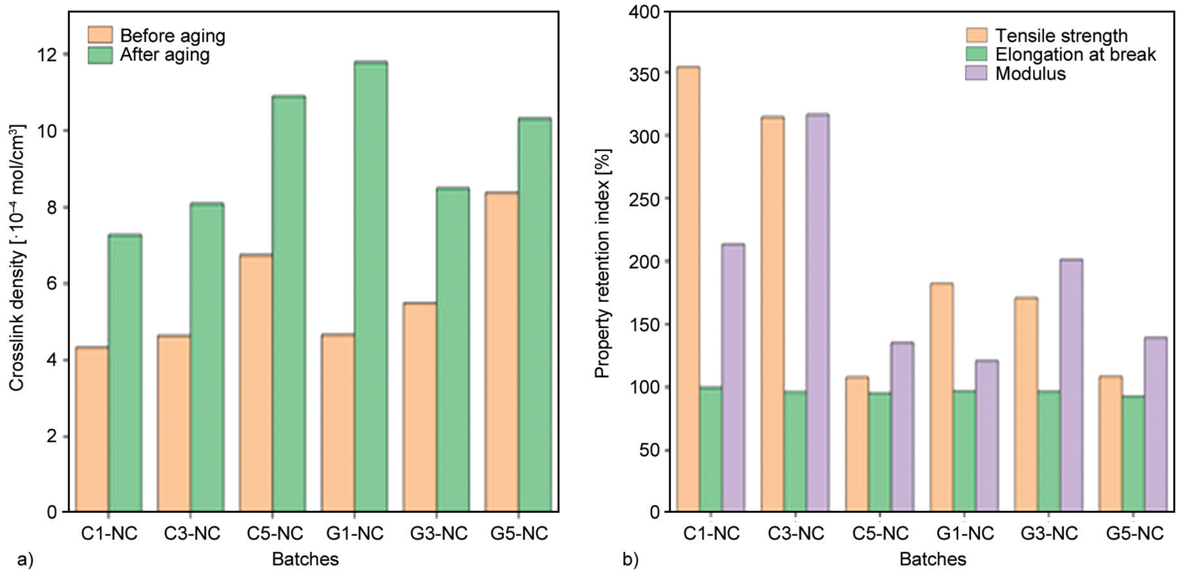

Figure 11. a) Crosslink density of composites after and before aging, b) mechanical properties after and before aging.

the crosslink density change. The change in mechanical properties was higher in the case of C_H ZnO-loaded C1-NC and C3-NC. This indicates that C1-NC and C3-NC exhibited more polysulfide than mono and disulfide linkages. At a loading of 5 phr of ZnO, the observed changes in C5-NC were minimal, indicating a higher presence of mono and disulfide linkages. Generally, the G ZnO-loaded G1-NC, G3-NC, and G5-NC exhibited minimal alterations in their mechanical properties as a result of their larger surface area. Previous studies have shown that a higher surface area and lower particle size of ZnO exhibit greater thermal stability due to its increased number of mono and disulfide linkages.

3.12. Magic triangle of rubber compounds – DMA and abrasion resistance analysis

Wet traction, rolling resistance, and abrasion resistance are the three primary factors determining tire rubber compounds' performance, collectively called the 'magic triangle'. Achieving enhancements in all three simultaneously is complex due to their interconnected nature. Striking a harmonious and simultaneous improvement in these characteristics remains an ongoing challenge for the tire industry. The rolling resistance and wet traction were observed from the tan delta vs. temperature peak, and the obtained traction and rolling resistance are listed in Table 5.

Table 5. Wet traction and rolling resistance from DMA analysis.

Sample designation	Wet traction (tan δ at 0 °C)	Rolling resistance (tan δ at 60 °C)
C1-NC	0.10742	0.12482
C3-NC	0.11080	0.10384
C5-NC	0.09301	0.06367
G1-NC	0.11058	0.10583
G3-NC	0.11160	0.08770
G5-NC	0.10866	0.07537

Rolling resistance were improved (decreased) by 15.2, 15.4%, in G1-NC, G3-NC compared to C1-NC, C3-NC and 18.5% increase G5-NC compared to C5-NC. Wet traction was increased by 3, 1, 16.8% in G1-NC, G3-NC, G5-NC compared to C1-NC, C3-NC, C5-NC.

The tan δ value at 60 °C is linked to the rolling resistance, and concurrent with measurements of cross-linking density, an increase in ZnO content correlates with an increase in compound cross-linking density. This increase is accompanied by a reduction in tan δ values, attributed to the cross-linking of rubber compounds, fostering improved synergistic motion and consequently diminishing friction between the polymer chains in the rubber. The G ZnO compounds showed significant improvements in abrasion resistance, and dynamic mechanical analysis gives optimum magic triangle properties compared to C_H ZnO compounds, as shown in Figure 12.

4. Conclusions

The current research has focused mainly on using these green-synthesized ZnO from sweet lime peel as an activator in rubber compounding. This approach provides a combination of simplicity, eco-friendliness, safety, reproducibility, and a high level

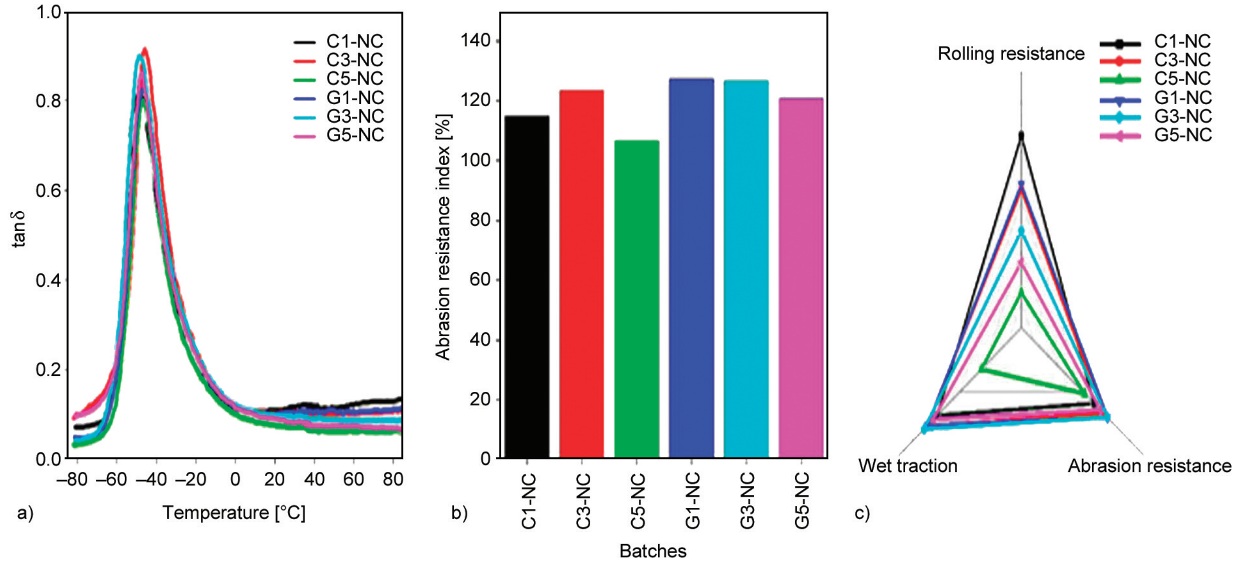

Figure 12. a) tan δ *vs.* temperature curve of composites, b) composites abrasion resistance index, c) extending magic triangle.

of stability. This research discusses the processes for the green and chemical synthesis of ZnO nanoparticles and the characterization of obtained nanoparticles. The main focus is applying green and chemically synthesized ZnO in natural rubber composites for use in tires. In addition, the study explores the cytotoxicity assessment of the prepared ZnO on mice cells. Sweet lime peel extract has been used to prepare green ZnO in a water medium. It was shown that the cytotoxicity of G ZnO is lesser in mice cells than C_H ZnO up to 25 µg/ml. Payne effect analysis was done on the composites prepared; it was shown that G ZnO-loaded composites exhibited a lower Payne effect, resulting in good polymer-filler interaction. This is reflected in the mechanical properties of the composites prepared. At 1, 3 or 5 phr of C_H ZnO or G ZnO were used for the study here; there was a 139% increase of tensile strength when compared C1-NC to G1-NC, where a 106 and 9% increase were observed while using G3-NC and G5-NC in place of C3-NC and C5-NC. Interestingly, G ZnO-loaded compounds achieved the tire's magic triangle properties, such as low rolling resistance, high wet traction, and high abrasion resistance, which are the key points of obtaining a magic triangle. Here, significant improvements in abrasion resistance compared to C_H ZnO with maintained wet traction and rolling resistance were obtained in the G3-filled compound. These results emphasize the promising potential of green ZnO as an environmentally friendly substitute for chemical ZnO in rubber compounding.

References

[1] Sarkar P., Bhowmick A. K.: Sustainable rubbers and rubber additives. Journal of Applied Polymer Science, **135**, 45071 (2018).
https://doi.org/10.1002/app.45701

[2] Öncel Ş., Ünügül T., Abacı U., Karaağaç B.: Coffee grounds as sustainable filler for bio-based rubber composites. Polymer Composites, in press (2024).
https://doi.org/10.1002/pc.28654

[3] Bardha A., Prasher S., Dumont M-J.: Waste biomass-derived rubber composite additives: Review of current research and future investigations into biowaste tire formulation. Biomass and Bioenergy, **183**, 107149 (2024).
https://doi.org/10.1016/j.biombioe.2024.107149

[4] Bernal-Ortega P., van Elburg F., Araujo-Morera J., Gojzewski H., Blume A.: Heading towards a fully sustainable tire tread compound: Use of bio-based resins. Polymer Testing, **133**, 108406 (2024).
https://doi.org/10.1016/j.polymertesting.2024.108406

[5] Xu H., Fan T., Ye N., Wu W., Huang D., Wang D., Wang Z., Zhang L.: Plasticization effect of bio-based plasticizers from soybean oil for tire tread rubber. Polymers, **12**, 623 (2020).
https://doi.org/10.3390/polym12030623

[6] Ayar M., Dalkiran A., Kale U., Nagy A., Karakoc T. H.: Investigation of the substitutability of rubber compounds with environmentally friendly materials. Sustainability, **13**, 5251 (2021).
https://doi.org/10.3390/su13095251

[7] Alam M. N., Kumar V., Park S-S.: Advances in rubber compounds using ZnO and MgO as *co*-cure activators. Polymers, **14**, 5289 (2022).
https://doi.org/10.3390/polym14235289

[8] Mostoni S., d'Arienzo M., Di Credico B., Armelao L., Rancan M., Dirè S., Callone E., Donetti R., Susanna A., Scotti R.: Design of a Zn single-site curing activator for a more sustainable sulfur cross-link formation in rubber. Industrial and Engineering Chemistry Research, **60**, 10180–10192 (2021).
https://doi.org/10.1021/acs.iecr.1c01580

[9] Mutukwa D., Taziwa R., Khotseng L. E.: A review of the green synthesis of ZnO nanoparticles utilising southern african indigenous medicinal plants. Nanomaterials, **12**, 3456 (2022).
https://doi.org/10.3390/nano12193456

[10] Agarwal H., Venkat Kumar S., Rajeshkumar S.: A review on green synthesis of zinc oxide nanoparticles – An eco-friendly approach. Resource-Efficient Technologies, **3**, 406–413 (2017).
https://doi.org/10.1016/j.reffit.2017.03.002

[11] Mostoni S., Milana P., Di Credico B., d'Arienzo M., Scotti R.: Zinc-based curing activators: New trends for reducing zinc content in rubber vulcanization process. Catalysts, **9**, 664 (2019).
https://doi.org/10.3390/catal9080664

[12] Anastas P., Eghbali N.: Green chemistry: Principles and practice. Chemical Society Reviews, **39**, 301–312 (2010).
https://doi.org/10.1039/b918763b

[13] Muthuvinothini A., Stella S.: Green synthesis of metal oxide nanoparticles and their catalytic activity for the reduction of aldehydes. Process Biochemistry, **77**, 48–56 (2019).
https://doi.org/10.1016/j.procbio.2018.12.001

[14] Rani S., Kumar P., Dahiya P., Dang A. S., Suneja P.: Biogenic synthesis of zinc nanoparticles, their applications, and toxicity prospects. Frontiers in Microbiology, **13**, 824427 (2022).
https://doi.org/10.3389/fmicb.2022.824427

[15] Ahmad N., Sharma S., Alam M. K., Singh V. N., Shamsi S. F., Mehta B. R., Fatma A.: Rapid synthesis of silver nanoparticles using dried medicinal plant of basil. Colloids and Surfaces B: Biointerfaces, **81**, 81–86 (2010).
https://doi.org/10.1016/j.colsurfb.2010.06.029

[16] Urnukhsaikhan E., Bold B-E., Gunbileg A., Sukhbaatar N., Mishig-Ochir T.: Antibacterial activity and characteristics of silver nanoparticles biosynthesized from *Carduus crispus*. Scientific Reports, **11**, 21047 (2021).
https://doi.org/10.1038/s41598-021-00520-2

[17] Frade T., Melo Jorge M. E., Gomes A.: One-dimensional ZnO nanostructured films: Effect of oxide nanoparticles. Materials Letters, **82**, 13–15 (2012).
https://doi.org/10.1016/j.matlet.2012.05.028

[18] Wahab R., Ansari S. G., Kim Y. S., Seo H. K., Kim G. S., Khang G., Shin H-S.: Low temperature solution synthesis and characterization of ZnO nano-flowers. Materials Research Bulletin, **42**, 1640–1648 (2007).
https://doi.org/10.1016/j.materresbull.2006.11.035

[19] Majid M., Hassan E-D., Davoud A., Saman M.: A study on the effect of nano-ZnO on rheological and dynamic mechanical properties of polypropylene: Experiments and models. Composites Part B: Engineering, **42**, 2038–2046 (2011).
https://doi.org/10.1016/j.compositesb.2011.04.043

[20] Qin X., Xu H., Zhang G., Wang J., Wang Z., Zhao Y., Wang Z., Tan T., Bockstaller M. R., Zhang L., Matyjaszewski K.: Enhancing the performance of rubber with nano ZnO as activators. ACS Applied Materials and Interfaces, **12**, 48007–48015 (2020).
https://doi.org/10.1021/acsami.0c15114

[21] Thomas S. P., Mathew E. J., Marykutty C. V.: Synthesis and effect of surface modified nano ZnO in natural rubber vulcanization. Journal of Applied Polymer Science, **124**, 3099–3107 (2012).
https://doi.org/10.1002/app.35349

[22] Sahoo S., Bhowmick K. A.: Influence of ZnO nanoparticles on the cure characteristics and mechanical properties of carboxylated nitrile rubber. Journal of Applied Polymer Science, **106**, 3077–3083 (2007).
https://doi.org/10.1002/app.24832

[23] Sreethu T. K., Das M., Parathodika A. R., Bhattacharya A. B., Naskar K.: Understanding the role of ZnO as activator in SBR vulcanizates: Performance evaluation with active, nano, and functionalized ZnO. Journal of Applied Polymer Science, **140**, 3077 (2023).
https://doi.org/10.1002/app.53257

[24] Sreethu T. K., Jana S., Jana N. R., Naskar K.: Influence of active, nano, and functionalized zinc oxide particles on the mechanical, cytotoxicity, and thermal stability of carbon black filled SBR/NR blends. Polymer Engineering and Science, **63,** 2354–2370 (2023).
https://doi.org/10.1002/pen.26381

[25] Kumbalaparambil S. T., Chandaparambil A. H., Naskar K.: *In-situ* formation of ZnO anchored silica: Sustainable replacement of conventional ZnO in SBR/NR blends. Express Polymer Letters, **17**, 1268–1285 (2023).
https://doi.org/10.3144/expresspolymlett.2023.96

[26] Susanna A., d'Arienzo M., Di Credico B., Giannini L., Hanel T., Grandori R., Morazzoni F., Mostoni S., Santambrogio C., Scotti R.: Catalytic effect of ZnO anchored silica nanoparticles on rubber vulcanization and cross-link formation. European Polymer Journal, **93**, 63–74 (2017).
https://doi.org/10.1016/j.eurpolymj.2017.05.029

[27] Susanna A., Armelao L., Callone E., Dirè S., d'Arienzo M., Di Credico B., Giannini L., Hanel T., Morazzoni F., Scotti R.: ZnO nanoparticles anchored to silica filler. A curing accelerator for isoprene rubber composites. Chemical Engineering Journal, **275**, 245–252 (2015).
https://doi.org/10.1016/j.cej.2015.04.017

[28] Thi T. U. D., Nguyen T. T., Thi Y. D., Thi K. H. T., Phan B. T., Pham K. N.: Green synthesis of ZnO nanoparticles using orange fruit peel extract for antibacterial activities. RSC Advances, **10**, 23899–23907 (2020).
https://doi.org/10.1039/d0ra04926c

[29] Darvishi E., Kahrizi D., Arkan E.: Comparison of different properties of zinc oxide nanoparticles synthesized by the green (using *Juglans regia* L. leaf extract) and chemical methods. Journal of Molecular Liquids, **286**, 110831 (2019).
https://doi.org/10.1016/j.molliq.2019.04.108

[30] Parathodika A. R., Naskar K.: Ultra-high molecular weight EPDM composites via crossover curing agents: Stabilized crosslink network structure and performance properties. Polymer Degradation and Stability, **219**, 110603 (2024).
https://doi.org/10.1016/j.polymdegradstab.2023.110603

[31] Parameswaran S. K., Bhattacharya S., Mukhopadhyay R., Naskar K., Bhowmick A. K.: Excavating the unique synergism of nanofibers and carbon black in natural rubber based tire tread composition. Journal of Applied Polymer Science, **138**, 49682 (2021).
https://doi.org/10.1002/app.49682

[32] Flory P. J., Rehner J.: Statistical mechanics of cross-linked polymer networks II. Swelling. The Journal of Chemical Physics, **11**, 521–526 (1943).
https://doi.org/10.1063/1.1723792

[33] Nielsen L. E.: Cross-linking–effect on physical properties of polymers. Journal of Macromolecular Science, Part C, **3**, 69–103 (1969).
https://doi.org/10.1080/15583726908545897

[34] Marzocca A. J.: Evaluation of the polymer-solvent interaction parameter χ for the system cured styrene butadiene rubber and toluene. European Polymer Journal, **43**, 2682–2689 (2007).
https://doi.org/10.1016/j.eurpolymj.2007.02.034

[35] Sreethu T. K., Naskar K.: Zinc oxide with various surface characteristics and its role on mechanical properties, cure-characteristics, and morphological analysis of natural rubber/carbon black composites. Journal of Polymer Research, **28**, 183 (2021).
https://doi.org/10.1007/s10965-021-02536-8

[36] Rao K. J., Kumaravel V., Pownraj I., Saha K., Korumilli T., Sadasivam S. K.: Biosynthesis and photocatalytic evaluation of ZnO nanoparticles using banana flower perianth. Journal of Cleaner Production, **380**, 135180 (2022).
https://doi.org/10.1016/j.jclepro.2022.135180

[37] Rasool A., Kiran S., Gulzar T., Abrar S., Ghaffar A., Shahid M., Nosheen S., Naz S.: Biogenic synthesis and characterization of ZnO nanoparticles for degradation of synthetic dyes: A sustainable environmental cleaner approach. Journal of Cleaner Production, **398**, 136616 (2023).
https://doi.org/10.1016/j.jclepro.2023.136616

[38] Gao Y., Xu D., Ren D., Zeng K., Wu X.: Green synthesis of zinc oxide nanoparticles using *Citrus sinensis* peel extract and application to strawberry preservation: A comparison study. LWT, **126**, 109297 (2020).
https://doi.org/10.1016/j.lwt.2020.109297

[39] Rasool K., Nasrallah G. K., Younes N., Pandey R. P., Abdul Rasheed P., Mahmoud K. A.: ‘Green’ ZnO-Interlinked chitosan nanoparticles for the efficient inhibition of sulfate-reducing bacteria in inject seawater. ACS Sustainable Chemistry and Engineering, **6**, 3896–3906 (2018).
https://doi.org/10.1021/acssuschemeng.7b04248

[40] Balanand S., Babitha K. B., Maria M. J., Mohamed A. A. P., Ananthakumar S.: Aqueous mechanical oxidation of Zn dust: An inventive technique for bulk production of ZnO nanorods. ACS Sustainable Chemistry and Engineering, **6**, 143–154 (2018).
https://doi.org/10.1021/acssuschemeng.7b01966

[41] Chandra R. D., Gopchandran K. G.: Simple, low-temperature route to synthesize ZnO nanoparticles and their optical neuromorphic characteristics. ACS Applied Electronic Materials, **3**, 3846–3854 (2021).
https://doi.org/10.1021/acsaelm.1c00471

[42] Zhou H., Li Z.: Synthesis of nanowires, nanorods and nanoparticles of ZnO through modulating the ratio of water to methanol by using a mild and simple solution method. Materials Chemistry and Physics, **89**, 326–331 (2005).
https://doi.org/10.1016/j.matchemphys.2004.09.006

[43] Prashanth G. K., Prashanth P. A., Bora U., Gadewar M., Nagabhushana B. M., Ananda S., Krishnaiah G. M., Sathyananda H. M.: *In vitro* antibacterial and cytotoxicity studies of ZnO nanopowders prepared by combustion assisted facile green synthesis. Karbala International Journal of Modern Science, **1**, 67–77 (2015).
https://doi.org/10.1016/j.kijoms.2015.10.007

[44] Malas A., Das C. K., Das A., Heinrich G.: Development of expanded graphite filled natural rubber vulcanizates in presence and absence of carbon black: Mechanical, thermal and morphological properties. Materials and Design, **39**, 410–417 (2012).
https://doi.org/10.1016/j.matdes.2012.03.007

[45] Marzocca A. J., Mansilla M. A.: Vulcanization kinetic of styrene-butadiene rubber by sulfur/TBBS. Journal of Applied Polymer Science, **101**, 35–41 (2006).
https://doi.org/10.1002/app.23173

[46] Akhlaghi S., Kalaee M., Mazinani S., Jowdar E., Nouri A., Sharif A., Sedaghat N.: Effect of zinc oxide nanoparticles on isothermal cure kinetics, morphology and mechanical properties of EPDM rubber. Thermochimica Acta, **527**, 91–98 (2012).
https://doi.org/10.1016/j.tca.2011.10.015

[47] Coran A. Y.: Chemistry of the vulcanization and protection of elastomers: A review of the achievements. Journal of Applied Polymer Science, **87**, 24–30 (2003).
https://doi.org/10.1002/app.11659

[48] Panampilly B., Thomas S.: Nano ZnO as cure activator and reinforcing filler in natural rubber. Polymer Engineering and Science, **53**, 1337–1346 (2013).
https://doi.org/10.1002/pen.23383

[49] Kim I-J., Kim W-S., Lee D-H., Kim W., Bae J-W.: Effect of nano zinc oxide on the cure characteristics and mechanical properties of the silica-filled natural rubber/butadiene rubber compounds. Journal of Applied Polymer Science, **117**, 1535–1543 (2010). https://doi.org/10.1002/app.31996

[50] Lee Y. H., Cho M., Nam J-D., Lee Y.: Effect of ZnO particle sizes on thermal aging behavior of natural rubber vulcanizates. Polymer Degradation and Stability, **148**, 50–55 (2018). https://doi.org/10.1016/j.polymdegradstab.2018.01.004

[51] Mostoni S., Milana P., D'Arienzo M., Dirè S., Callone E., Cepek C., Rubini S., Farooq A., Canevali C., Di Credico B., Scotti R.: Studying stearic acid interaction with ZnO/SiO_2 nanoparticles with tailored morphology and surface features: A benchmark for better designing efficient ZnO-based curing activators. Ceramics International, **49**, 24312–24321 (2022). https://doi.org/10.1016/j.ceramint.2022.12.013

[52] Pimolsiriphol V., Saeoui P., Sirisinha C.: Relationship among thermal ageing degradation, dynamic properties, cure systems, and antioxidants in natural rubber vulcanisates. Polymer – Plastics Technology and Engineering, **46**, 113–121 (2007). https://doi.org/10.1080/03602550601152861